NJC

PAPER

View Article Online
View Journal | View Issue

Cite this: *New J. Chem.*, 2016, **40**, 5432

Effect of a chelating agent at different pH on the spectroscopic and structural properties of microwave derived hydroxyapatite nanoparticles: a bone mimetic material

Vijay Kumar Mishra,[a] Birendra Nath Bhattacharjee,[b] Devendra Kumar,*[b] Shyam Bahadur Rai*[a] and Om Parkash[b]

In the present investigation, the effect of a capping agent (EDTA) and pH on the optical and structural characteristics of HAp nanoparticles (NPs) has been studied. Six samples of HAp were synthesized under six different chemical conditions. The HAp specimens were prepared *via* a microwave irradiation technique (MWIT) in the presence and absence of EDTA at three different pH values 9, 11 and 13. All the samples were calcined at 900 °C. HAp NPs with different sizes and shapes were found to be developed. X-ray diffraction (XRD), scanning electron microscopy (SEM) and transmission electron microscopy (TEM) techniques were employed to determine the crystal structure, crystallite size and bonding parameters of the resulting HAp. The SEM measurements revealed the formation of the different morphologies of the HAp NPs under different physico-chemical conditions. Electron microscopies revealed that the particle size of the samples was in the range of ~10–200 nm. The TEM results were in good agreement with the SEM results. The study revealed the vital role of the chelating agent (EDTA) in the formation of the pure phase HAp nanostructures. EDTA assisted the formation of needle-like nanorods of HAP and prevented agglomeration. EDTA also prevented carbonate impurities. Carbonate impurities, probably from the atmosphere, were observed in the HAp samples formed without EDTA. Despite the effect of EDTA, the pH of the solution also played a key role in deciding the final morphology of the HAp nanostructures. The samples were also characterized spectroscopically using Fourier transform infrared (FT-IR) spectroscopy and Raman techniques to understand the molecular interactions. The application of laser induced breakdown spectroscopy (LIBS) detected the presence of N and further confirmed the formation of the HAp powders.

Received (in Montpellier, France) 24th November 2015,
Accepted 11th April 2016

DOI: 10.1039/c5nj03322e

www.rsc.org/njc

1. Introduction

Hydroxyapatite ($Ca_{10}(PO_4)_6(OH)_2$; HAp) is chemically similar to the inorganic part of mammalian hard tissues. It has attracted considerable attention of scientists due to its excellent biocompatibility and similarity with natural bone and teeth tissues.[1,2] HAp has an excellent ability to form chemical bonds to the host's bone tissues. It also shows marvelous compatibility with hard tissues as well as skin and other soft tissues of muscles without any toxic effects.[3] The bioactivity of HAp depends on several factors such as the morphology of the material, crystal size, Ca/P ratio, presence of ions (carbonate, magnesium, strontium, sodium *etc.*), morphology and the texture of the biomaterial.[3,4] Since, the clinical applications of HAp are strongly dependent on the morphology and crystal size of pure phase HAp, hence considerable attention and efforts have been focused on these factors.[5,6] Huang *et al.* (2015) reported a Cu-substituted carbonated hydroxyapatite coating, which has good antibacterial efficacy and corrosion resistance with no cytotoxicity.[7] However, Ding *et al.* (2015) showed cytocompatibility and corrosion resistance of zinc-doped hydroxyapatite coatings on a titanium substrate.[8] The crystallographic properties and surface morphology of HAp widely depend on the preparation routes followed, different resources and starting reagents used and dopants.[6,9] It was believed that a suitable morphology having nanoscale size will facilitate the improved applications in different areas of bone strengthening, bone healing, osteoporosis and other bone functions.

The use of nanostructured HAp as a drug vehicle/carrier in drug delivery/targeted drug delivery/gene delivery/bioimaging is

[a] *Department of Physics, Centre of Advanced Studies, Institute of Science, Banaras Hindu University, 221005, India. E-mail: sbrai49@yahoo.co.in, vijaybioceramic@gmail.com; Fax: +91-542-2368174, +91-542-2369889; Tel: +91-542-6701793, +91-542-2307308*

[b] *Department of Ceramic Engineering, Indian Institute of Technology, Banaras Hindu University, 221005, India. E-mail: devendra.cer@itbhu.ac.in*

one of the latest applications of HAp NPs. It has also been reported that the different nanostructures/morphologies of HAp have different drug loading efficiencies for a particular drug.[10] Therefore, the drug loading efficiency of HAp for a particular drug may be enhanced or controlled by developing a particular nanostructure of HAp. HAp NPs have been widely employed in delivery systems for antibiotics,[11] genes[12,13] proteins[14] and various drugs[15,16] due to their excellent biocompatibility and non-toxicity. Recently, Guo *et al.* (2012) reported the formation of micro and mesoporous carbonated HAp microspheres with good drug loading efficiency and *in vitro* investigations on the drug's stability.[17] The selection of suitable morphology, size and shape of HAp NPs for an efficient loading of a particular drug used for a specific disease is still a challenge for scientists. Therefore, the development of different nanostructures with a controlled morphology of pure phase HAp was not only desirable but was also necessary. In order to develop various morphologies/nanostructures of HAp, a lot of efforts have been made. HAp with a slight doping of a non-reacting metal has been found to affect the morphology of HAp nanostructures drastically.[18] There are several methods, such as sol–gel,[19] low temperature synthesis-modified sol–gel technique,[20] homogeneous precipitation/co-precipitation,[21,22] hydrothermal,[23] mechano-chemical,[24] ultrasonic spray freeze-drying,[25] spray dry,[26] combustion synthesis,[27] emulsion techniques,[28] radio frequency plasma spray[29] and microwave irradiation techniques,[30–34] have come up in recent years to synthesize HAp. Some biological resources *viz.* coral skeletal carbonate *via* hydrothermal exchange[35] and hen's egg shell *via* precipitation[36] methods have also been used to prepare HAp powders. Among these, the microwave irradiation technique was found to be very quick, efficient and eco-friendly to prepare pure phase of HAp nanoparticles.[37] Another interesting thing is that the morphology of the HAp nanostructures can be controlled easily using suitable microwave power[2] as well as calcination temperatures.[30]

A slight change in one or more physical and/or chemical condition(s) in a controlled manner can cause a change in the final morphology, crystal size and shape of HAp NPs. The power of the microwave radiation, duration of radiation (microwave on–off working cycle and total microwave exposure time), temperature of the synthesis as well as calcination/annealing/sintering temperature are some of the basic physical parameters that can be tuned with different combinations to control the morphology of HAp nanostructures.[2,18,31] The presence of a chelating agent (EDTA, CTAB, *etc.*), pH value of the solution and initial ingredients (starting reagents) are the chemical parameters that need to be controlled to obtain the desired morphology of HAp NPs.

The present study is focused on the effect of the chemical conditions varying by the presence and absence of a capping (chelating) agent (EDTA) at different pH values (9, 11 and 13) on the final morphology, crystal shape and size of the HAp nanostructures derived *via* a microwave irradiation synthesis route. The present study has potential applications in biomedical engineering because different morphologies with different properties directly affect the bioactivity/biocompatibility/drug loading capacity of HAp on the implantation or administration in host natural soft and hard tissues. The different nanostructures of HAp powders are also useful in bone graft materials, bone cement and coating materials for bone implants.

2. Experimental procedures

2.1. Sample preparation

All the chemicals, calcium nitrate tetrahydrate, diammonium hydrogen phosphate and EDTA, were purchased from LOBA Chemie with high purity (>99%) and were used directly without any further purification. Ethylene diamine tetraacetic acid (EDTA; $C_{10}H_{16}N_2O_8$) served the purpose of the capping/complexing agent. In the present investigation, six samples of HAp precursor powders at three different pH values 9, 11 and 13 were prepared *via* a microwave irradiation technique (MWIT). First three samples were prepared in the presence of EDTA at pH 9, 11 and 13, whereas the other three samples were prepared without EDTA at the same pH values of 9, 11 and 13. The detailed description and procedure for the synthesis of the precursor powder at pH 9 is reported by Mishra *et al.* (2014).[30] The procedure was replicated for pH 11 and 13 controlled by NaOH pellets for rest of the two EDTA assisted samples. The procedure was again replicated for each of pH value in the absence of EDTA. Finally, lime white fine powders called HAp precursor materials at pH 9 were obtained.[18] All the HAp precursor powders were calcined at 900 °C *via* a very slow heating rate of 1 °C min^{-1} for the elimination of impurities and formation of fine crystallized HAp. The white color fine powder samples thus obtained were processed using X-ray diffraction and electron microscopy techniques to verify the formation of nanoscale HAp. Spectroscopic characterizations using FT-IR, Raman and LIBS techniques were then carried out to confirm the formation of HAp.

2.2. Sample characterizations

In order to investigate the structural and morphological changes that occurred in the HAp nanoparticles upon changing the chemical conditions of preparation, structural and optical techniques were used. The phase contribution was decided by XRD (Rigaku Desktop Miniflex II X-Ray Diffractometer, equipped with Ni filter and the CuKα radiation). The surface morphologies of the nanostructured HAp powders were disclosed using SEM (Inspect S-50, FEI USA (SEA) PTE Ltd, Singapore, FP 2017/12). Transmission electron microscopy (TEM, FEI, TECNAI-G^2) at an accelerating voltage of 200 kV was used. The powder samples were dispersed into acetone and sonicated for an hour and one drop of this well dispersed suspension was placed upon a carbon coated copper grid. The process was replicated for the other samples. The molecular structures of the precursor and other calcinated powders were studied using Fourier transform infrared spectroscopy (Perkin Elmer spectrum 65, FT-IR) between 4000 and 400 cm^{-1}. The samples were diluted using KBr (materials : KBr = 1 : 10) to form pellets for IR spectroscopy. The FT-IR technique confirmed the formation of HAp in all the samples. The LIBS experimental arrangement employed here is shown in ref. 38. It consists of a laser source, a rotational

stage (Sandvic Components, India) placed on a jack (Sandvic Components, India) to provide concentric rotation of the sample and a spectrometer equipped with a detector. A Nd:YAG laser (532 nm) (continuum surelite III-10) was employed as a laser source with the capability of delivering a highest energy of 425 mJ. The pulse duration (FWHM) is 4 ns with a maximum pulse repetition rate of 10 Hz. The LIBS spectra of the samples were obtained in the spectral range of 200–500 nm with 0.1 nm spectral resolution. The laser pulsed energy was measured using an energy meter (Genetec-e model UP19K-30H-VM-DO).

3. Results and discussion

3.1. Spectroscopic characterization

3.1.1. Fourier transform infrared (FT-IR) spectroscopy. Fig. 1(a–f) illustrates the FT-IR spectra of the six HAp samples formed under the six different physico-chemical conditions. HAp samples (a), (b) and (c) were prepared at three different pH values 9, 11 and 13, respectively in the presence of EDTA whereas, samples (d), (e) and (f) were prepared accordingly at the same pH values 9, 11 and 13 without using EDTA.

The calcination temperature for all the samples was kept at 900 °C. All the physical conditions *viz.* power as well as time duration of microwave exposure, on–off working cycle, calcination temperature and duration (calcinations dynamics) were kept the same for all the samples. The IR and Raman active bands observed in these samples are shown along with their assignments in Table 1. IR spectroscopy confirmed the formation of HAp under different physico-chemical conditions. The FT-IR spectra of HAp powders prepared under different conditions show a large number of bands corresponding to the different modes of vibrations of the various functional groups present. An absorption band observed at 1430 cm^{-1} was weak in the IR patterns (a–c) of the samples formed using EDTA. This band was attributed to ν_3 symmetric stretching of carbonate ions (CO_3^{2-}). This band was shifted to 1450 cm^{-1} in

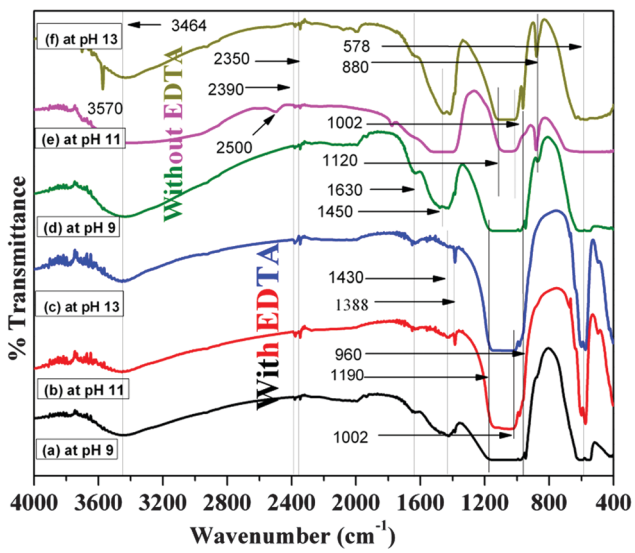

Fig. 1 FT-IR spectra of the HAp powder samples prepared at pH (a) 9, (b) 11 and (c) 13 with EDTA and at pH (d) 9, (e) 11 and (f) 13 without EDTA.

Table 1 The IR and Raman bands observed in HAp samples (a–c) prepared in the presence of EDTA and samples (d–f) prepared in the absence of EDTA at pH 9, 11 and 13

FT-IR active bands at wavenumber (cm^{-1})						Raman active bands at wavenumber (cm^{-1})						Assignments symmetric/asymmetric bending/stretching
HAp prepared with EDTA at pH			HAp prepared without EDTA at pH			HAp prepared with EDTA at pH			HAp prepared without EDTA at PH			
(a) 9	(b) 11	(c) 13	(d) 9	(e) 11	(f) 13	(a) 9	(b) 11	(c) 13	(d) 9	(e) 11	(f) 13	
—	—	—	—	—	—	460	—	—	—	—	—	ν_2 symmetric bending mode of O–P–O in PO_4^{3-}
578	578	578	578	—	578	—	—	—	—	—	—	ν_4 asymmetric bending mode of O–P–O in PO_4^{3-}
—	—	—	880	880	880	—	—	—	—	—	—	ν_2 carbonate ions (CO_3^{2-})
960	960	960	960	960	960	965	965	965	965	965	965	ν_1 symmetric stretching mode of P–O in PO_4^{3-}
—	1002	1002	—	1002	1002							ν_3 asymmetric stretching of P–O in PO_4^{3}
1002–1190	1002–1190	1002–1190	1002–1190	1002–1190	1002–1120	1120	1120	1120	1120	1120	1120	ν_3 asymmetric stretching of P–O in PO_4^{3}
—	1388	1388	1388	1388	1388	—	—	—	—	—	—	ν_1 symmetric stretching (CO_3^{2-}) vibrational band
1430	1430	1430	1450	1450	1450	—	—	—	—	—	—	ν_3 carbonate ions (CO_3^{2-})
1630	1630	1630	1630	1630	1630	—	—	—	—	—	—	ν_2 bending mode of H–O–H in lattice H_2O
2350	2350	2350	2350	2350	2350	—	—	—	—	—	—	ν_3 asymmetric stretching of carbonate ions (CO_3^{2-})
2390	2390	2390	2390	2390	2390	—	—	—	—	—	—	ν_3 asymmetric stretching of carbonate ions (CO_3^{2-})
—	—	—	—	2500	—	—	—	—	—	—	—	Stretching mode of the OH^-
3464	3464	3464	3464	3464	3464	—	—	—	—	—	—	Stretching mode of lattice H_2O
—	—	—	—	—	3570	—	—	—	—	—	—	Symmetric stretching mode of the OH^-

the IR spectra (d–f) of samples formed without EDTA and has strong intensities. Another weak band observed at 1388 cm^{-1} in the EDTA assisted as well as without EDTA assisted samples was due to the ν_1-symmetric stretching band of carbonate (CO_3^{2-}) impurities.

It was interesting to note that the intensity of this band in the infrared spectra of samples (a–c) decreases with an increase in the pH value. However, in samples (d–f) in which EDTA was not used, the intensity also increased with the pH value of the solution. Two weak but sharp shoulders seen at 2350 and 2390 cm^{-1} in the IR spectra of all the samples (a–f) were assigned to the ν_3-asymmetric stretching of carbonate (CO_3^{2-}) impurities.

Carbonate should not be present in pure HAp; however, its presence was expected to be due to its absorption from the atmosphere during sample preparation,[39,40] which could not be avoided under normal synthesis conditions. However, it could be reduced by increasing the pH in the presence of EDTA. An additional sharp band noticed at 880 cm^{-1} in the IR spectra of samples (d–f) formed without EDTA was due to the ν_2-vibration of carbonate ions. Its intensity increases with an increase in the pH of the solution. This band was absent in the EDTA assisted HAp ν_2-vibration of carbonate ions. This band was absent in EDTA assisted HAp samples. The presence of this additional band due to carbonate impurities in the HAp samples formed without EDTA confirms the superiority of the EDTA assisted HAp samples over the samples formed without EDTA. This clearly shows that EDTA prevents the carbonate impurities to be attached during the synthesis. The most plausible reason for the merit of EDTA may be understood on the basis of its complex forming ability. Being a chelating agent, EDTA may have shielded the sites for carbonate ions to be attached. Thus, on the basis of the IR studies, we can say that EDTA plays a vital role in forming pure phase HAp nanostructures.

Strong absorption bands appearing between 950 and 1200 cm^{-1} were the characteristic stretching bands of O–P–O in PO_4^{3-} of HAp. A shoulder was noticed at 578 cm^{-1} and assigned to the ν_4-asymmetric bending mode of O–P–O. This band was comparatively sharp in (a–c) but appears broad in (d–f), showing again the superiority of the EDTA assisted HAp. From these studies, it was concluded that EDTA played an important role in the formation of pure HAp. A strong (characteristic) band at 960 cm^{-1} was noticed in all the spectra of the HAp samples and was attributed to the ν_1-symmetric stretching mode of P–O in PO_4^{3-}. An envelope between 1002 and 1120 cm^{-1} preferably in (e) and (f) was attributed to the ν_3-asymmetric stretching of P–O, whereas in samples (a–d), this spreading was found to be more at 1002–1190 cm^{-1} due to superposition of the band at 1180/1190 cm^{-1}. The broad envelope centered at 3464 cm^{-1} and a weak shoulder at 1630 cm^{-1} were assigned to ν_1-stretching and ν_2-bending mode of H–O–H (water molecule), respectively, present in the lattice (30, 31, 40). A sharp shoulder band at 3570 cm^{-1} in the IR spectrum of (f) was assigned to the symmetric stretching mode of the OH^- ions. It was interesting to note that no band due to the ν(C–H) stretching mode was seen in the IR spectrum of any of these samples. The absence of ν(C–H) stretching bands between 2800 and 3000 cm^{-1} in the IR spectra of the samples clearly indicate the complete removal of EDTA content from the powder samples (particularly in samples containing EDTA) during washing and the rest during calcination at 900 °C.

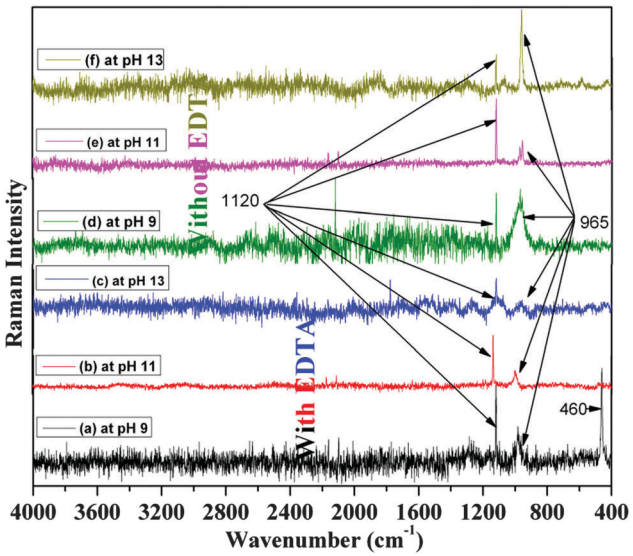

Fig. 2 Raman spectra of HAp powder samples prepared at pH (a) 9, (b) 11 and (c) 13 with EDTA; and at pH (d) 9, (e) 11 and (f) 13 without EDTA.

3.1.2. Raman spectroscopy. The Raman spectra of the HAp samples formed with and without EDTA at different pH values are shown in Fig. 2(a–f). Fig. 2(a–c) shows the Raman spectra of the HAp samples prepared at pH 9, 11 and 13 in the presence of EDTA. However, Fig. 2(d–f) show the Raman spectra of the HAp samples formed at pH 9, 11 and 13 in the absence of EDTA. A strong peak appearing at 460 cm^{-1} in the Raman profile of sample (a) was assigned to the ν_2 symmetric bending mode of O–P–O in PO_4^{3-}. This peak does not appear in the Raman spectra of other samples as well as in the IR of any of the samples studied. A peak was noticed at 965 cm^{-1} in all the HAp samples (a–f) and was attributed to the ν_1 symmetric stretching mode of P–O in PO_4^{3-}. The intensity of this band decreases in (a–c) with an increase in the pH value of the samples. No peak due to carbonate ions was seen in Raman spectra of any of these samples.

A sharp peak at 1120 cm^{-1} appears in the Raman spectra of all the samples (a–f) and was assigned to the ν_3 asymmetric stretching vibration of P–O in PO_4^{3-}. The intensities of all the Raman bands decrease with an increase in the pH value of the final solution. The Raman technique confirms again the formation of HAp.

3.1.3. Laser induced breakdown spectroscopy (LIBS). The LIBS technique was used to qualitatively identify the elements present in the samples. The samples were taken in the pellet form; however, any type of sample (solid, liquid and gas) can be monitored by LIBS. The LIBS spectra of two HAp samples prepared at pH 9 in the presence and absence of EDTA and calcined at 900 °C have been studied and samples were shown

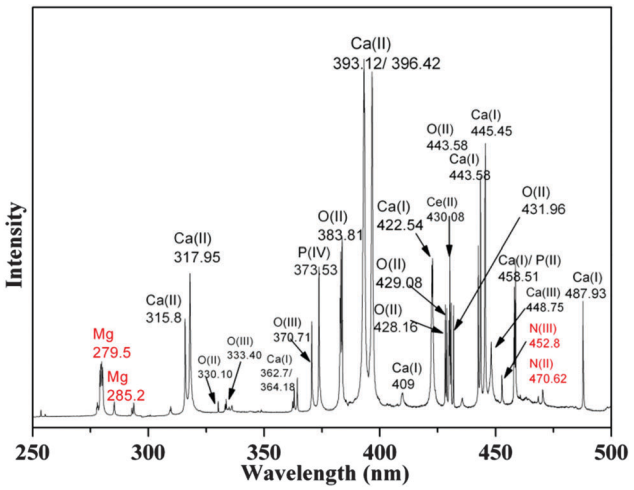

Fig. 3 The laser induced breakdown spectrum (LIBS) of the HAp powder sample prepared with EDTA at pH 9 and calcined at 900 °C.

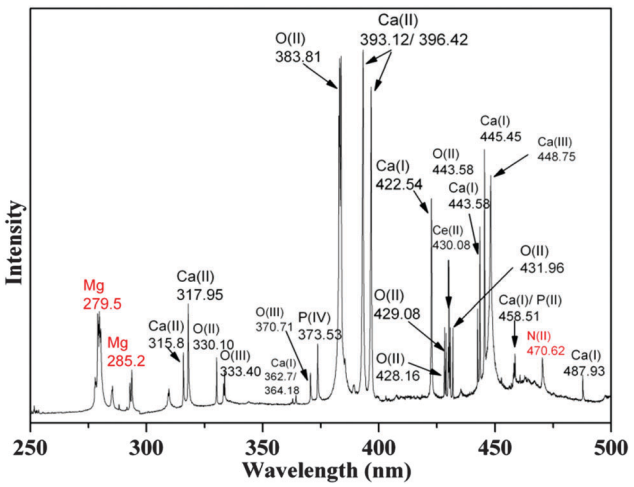

Fig. 4 The laser induced breakdown spectrum (LIBS) of the HAp powder sample prepared without EDTA at pH 9 and calcined at 900 °C.

in Fig. 3 and 4, respectively. The spectral lines have been identified using the National Institute of Standards and Technology atomic optical database (111-NWAST)[41] and are shown in Table 2.

The spectral lines for Ca, P and O have been identified and listed in Table 2. These lines show the formation of HAp very clearly. Some Mg as well as N impurity (probably due to chemicals) was also detected in the LIBS spectra. Mg lines at 279.5 and 285.2 were common to both the spectra of HAp derived with EDTA and without EDTA. However, the LIBS pattern of HAp formed with EDTA contains an additional line for N at 452.8 nm. This may be present due to chemical impurity and not due to the presence of EDTA. An EDTA molecule cannot exist at higher temperatures at which HAp was calcined. LIBS detects the atom(s) not molecule of the impurity. This impurity was present at an atomic level due to chemicals that may not be eliminated easily until we further purify the chemicals after purchase.

Table 2 Laser induced breakdown spectral (LIBS) lines with their assignments

LIBS spectral line position (nm)		
With EDTA	Without EDTA	Assignment
279.5	279.5	Mg
285.2	285.2	Mg
315.8	315.8	Ca(II)
317.95	317.95	Ca(II)
330.10	330.10	O(II)
333.40	333.40	O(III)
362.7	362.7	Ca(I)
364.18	364.18	Ca(I)
370.71	370.71	O(III)
373.53	373.53	P(IV)
383.81	383.81	O(II)
393.12	393.12	Ca(II)
396.42	396.42	Ca(II)
409	409	Ca(I)
422.54	422.54	Ca(I)
428.16	428.16	O(II)
429.08	429.08	O(II)
430.08	430.08	Ce(II)
431.96	431.96	O(II)
443.58	443.58	Ca(I)/O(II)
445.45	445.45	Ca(I)
448.75	448.75	Ca(III)
452.8	—	N(III)
458.51	458.51	Ca(I)/P(II)
470.62	470.62	N(II)
487.93	487.93	Ca(I)

3.2. Structural characterizations

3.2.1. X-ray diffraction (XRD) analysis. The X-ray diffraction patterns of all six HAp samples (a–f), grown under different chemical conditions, are shown in Fig. 5. The diffraction patterns (a), (b) and (c) correspond to the samples formed at pH 9, 11 and 13 with EDTA, respectively, whereas (d), (e) and (f) were without EDTA. A glance on patterns (a) to (f) revealed clearly the formation of hydroxyapatite in all the chemical conditions used. All the peaks observed in the patterns were

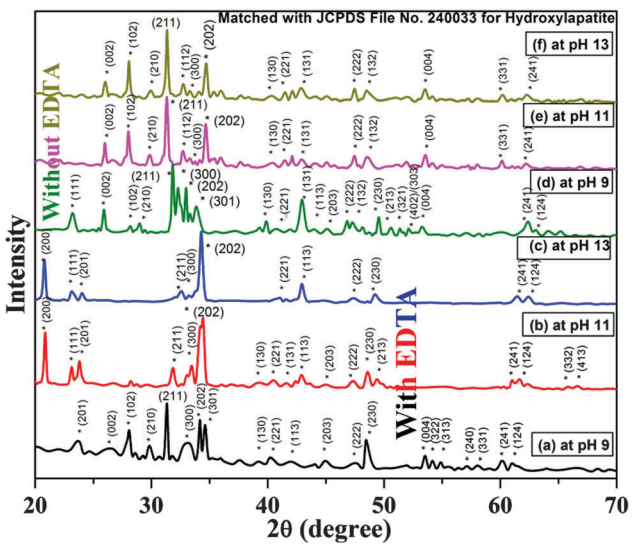

Fig. 5 The XRD patterns of the HAp powder samples prepared at pH (a) 9, (b) 11 and (c) 13 with EDTA, and at pH (d) 9, (e) 11 and (f) 13 without of EDTA.

in good agreement with the JCPDS File (24-0033) for hydroxyapatite (HAp).

If we compare the XRD patterns for samples (a), (b) and (c) prepared with EDTA at pH 9, 11 and 13, the number of XRD peaks noticed between 25–30 and 50–60 degree in (a) were not seen in (b) and in (c). Moreover, as the pH of the HAp precursor solution was increased, the intensity of the prominent HAp peaks such as (211) and (230) planes was found to decrease and for the peaks corresponding to the (202) and (113) planes were significantly increased. Peaks due the diffraction planes (301) and (102) were observed in pattern (a) and were completely vanished in (b) and (c) as the pH was increased. Some new peaks for HAp due to diffraction by the (200) and (111) planes started to appear in pattern (b) and become more prominent in (c). The crystallite sizes in these powder samples lie in the range of 25–45 nm. On the other hand, the XRD pattern of samples (d–f) reveals that the peak due to the (111) plane appearing in (d) nearly vanished in (e) and (f). The intensity of the peaks due to (002), (131), (300), (230) and (241) also decreased considerably at higher pH values. The peaks due to the planes (200), (201) appearing in EDTA assisted samples were not seen in the samples formed without EDTA.

Another interesting feature was that there was a small peak shift in the XRD profiles in the EDTA assisted samples. Thus, the prominent HAp (211), (300), (202) and (301) peaks in the XRD patterns of samples (a), (b) and (c) were found to be slightly shifted towards higher angle side when compared to the XRD patterns of samples (d), (e) and (f). Hike/suppression/appearance/vanishing in the peak intensity may be understood on the basis of the atomic structure factor. These changes in the peak intensity occur due to the presence of impurity element(s) in the samples (a–c). Each element of EDTA contributes to the atomic structure factor, positive or negative, for a particular diffraction plane, which affects the peak intensity as well as the peak position. The X-ray peak shift may be due to three basic reasons, (i) the lattice parameter change, (ii) the presence of residual stress and (iii) the defect concentration.[30,42] In the present case, the peak shift seems due to the second reason; the presence of residual stress (some impurity element) as nitrogen was also revealed also the LIBS technique. Some impurities may not be eliminated even up to 1000 °C. In order to eliminate these, a heat treatment above this temperature was needed. The contribution of nitrogen, positive or negative, consequents these peak shifts.

3.2.2. Scanning electron microscopy (SEM). Fig. 6(a–d) show some additional SEM images of four HAp samples prepared under four different physico-chemical conditions. Sample (a) and (b) were the HAp precursor powders prepared using EDTA at pH values 9 and 13, respectively. Images (c) and (d) were the microstructures of the samples obtained during calcination of the HAp precursor powder (a) at 600 and 900 °C, respectively.

The SEM image of the HAp precursor (a) shows needle/strip-like nanostructures. The width of the nanostrips formed in the HAp precursor (a) was around 50 nm. The HAp powder sample calcined at 600 °C shows almost no change in the surface morphology, as shown in image (c). It shows needle-like nanostructures of 45 nm width. As shown in micrograph (d), the morphology of the HAp powder sample was changed drastically upon heating at 900 °C. The needle-like nanostructures get converted into capsule-like nanostructures with an average

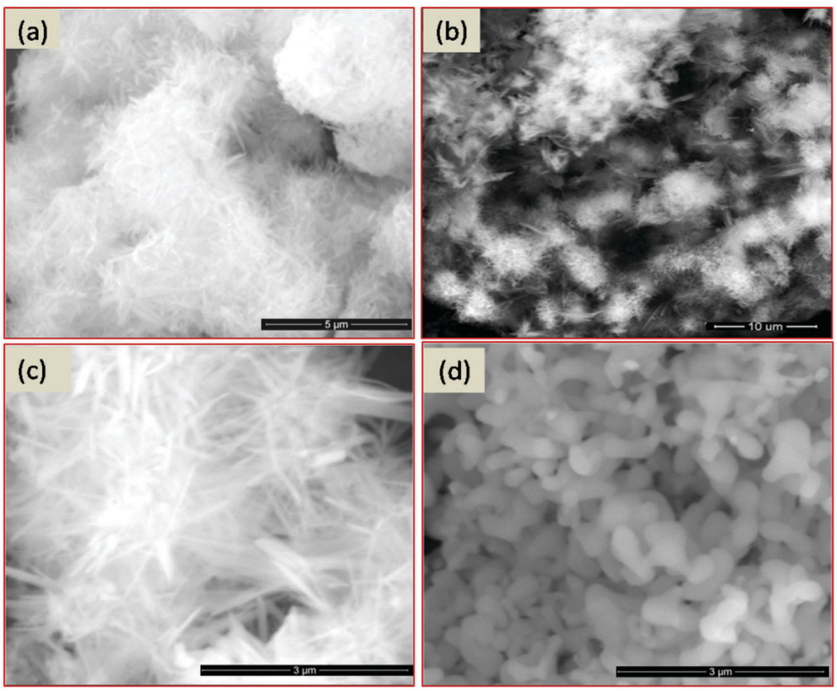

Fig. 6 SEM images of the HAp precursor powders at pH (a) 9 and (b) 13, and the HAp powders obtained upon calcination at (c) 600 °C and (d) 900 °C using precursor powder (a).

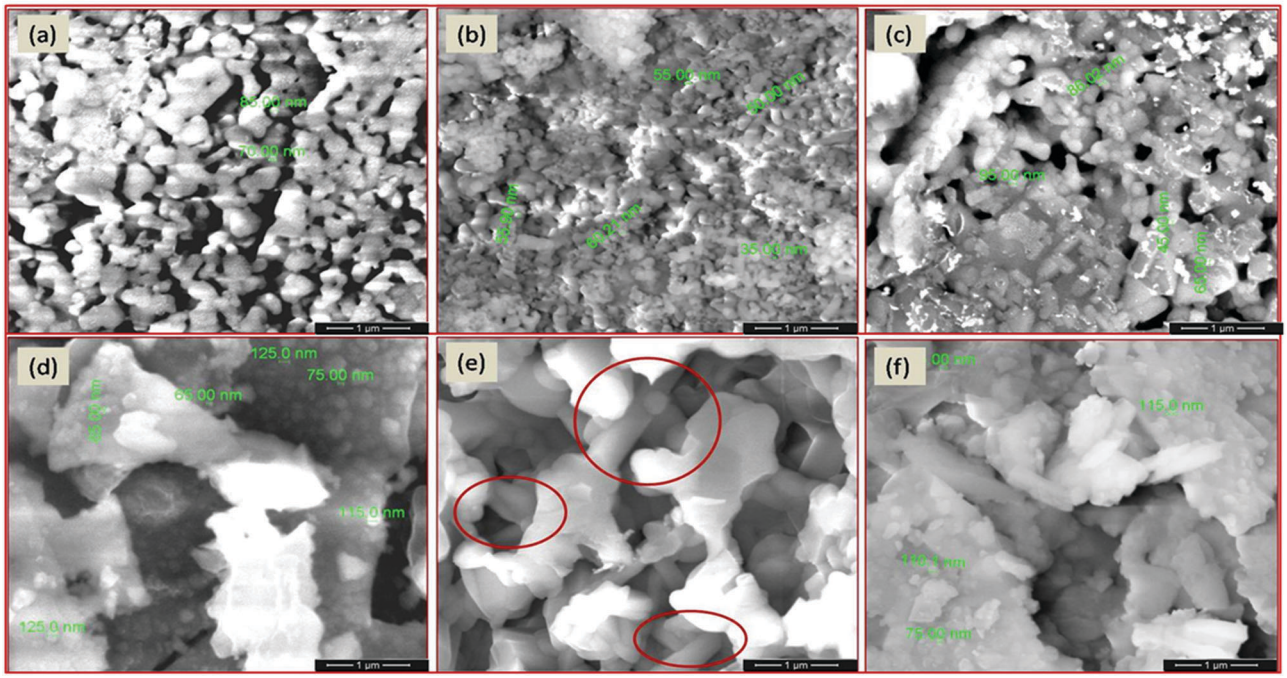

Fig. 7 SEM images of the HAp powder samples prepared at pH (a) 9, (b) 11 and (c) 13 using EDTA, and (d) 9, (e) 11 and (f) 13 without EDTA, calcined at 900 °C.

diameter of ~200 nm upon heating at 900 °C. A careful examination of image (c) revealed some flower-like morphology of the HAp nanostructures at pH 13. Some bunches of nanostrips/needles/rods have been found to grow together under the applied conditions. These images uncover the effect of pH and calcination temperature on the surface morphology of the HAp powders prepared *via* the microwave irradiation technique.

The micrographs (at 1 μm magnification) shown in Fig. 7(a–f) exhibit the simultaneous effect of pH and EDTA (a chelating/capping agent/surfactant) on the surface morphology of the HAp powders prepared *via* microwave irradiation under ambient physico-chemical conditions and calcined at 900 °C. Microstructures (a) to (c) show capsules/spheres/ellipsoids-like homogeneous NPs of HAp grown under calcination at 900 °C.

The surface morphologies of these samples at their precursor (as synthesized) stage and even up to 600–700 °C show a needle/rod-like structure of NPs (see Fig. 6(a and c)). When the samples were calcined at 900 °C, the morphologies of the samples were totally changed (see Fig. 7(a–f)). The particle sizes of the nanostructures were under 100 nm in sample (a) and (c). However, in sample (b), this value was ~35–60 nm, which was much less than (a) and (c). The morphology of (b) was comparatively more homogeneous and dense capsule-like nanostructures similar to those shown in Fig. 6(d). The images (d), (e) and (f) show the surface morphologies of HAp powders prepared at pH 9, 11 and 13, respectively, *via* the microwave irradiation route without EDTA and calcined at 900 °C. All the physico-chemical conditions for the preparation of samples (a–c) were same as in (d–f). From a careful comparison of images (d and f), we find that the size of the HAp NPs was around 100 nm and were strongly embedded into the clusters of several micrometers. The image of (e) shows slightly different microstructures, *i.e.* rod-like (in rings), as shown in Fig. 7. The diameter of the rod-like microstructures was a fraction of a micrometer and their length may be several micrometers. The effects of EDTA at a certain pH and calcination temperature are obvious and may be understood using Fig. 6(a–d) and the corresponding micrographs in Fig. 7(a–f). The particle size in images (d–f) was much larger than the particle size shown in micrographs (a–c) due to agglomeration of the HAp particles. Therefore, we can say that EDTA prevents agglomeration of the particles. The effect of pH on the surface morphology of HAp was clear from Fig. 6. Flower-like shapes containing needle/rod/strip-like nanostructures were obtained at higher pH values. The nanorod-like morphology of HAp calcium phosphate gets converted into capsule-like nanostructures due to their diffusion at a temperature near 900 °C. This shows a clear-cut effect of calcination/annealing/sintering temperature on the surface morphology of HAp. A detailed study on the effect of calcination/annealing/sintering temperatures on the surface morphology of HAp has already been carried out and discussed by Mishra *et al.* (2014).[30]

3.2.3. Transmission electron microscopy (TEM). TEM micrographs of the HAp powder samples prepared without using EDTA and with EDTA as a capping agent are shown in Fig. 8(a) and (b), respectively. Both these samples were prepared at pH 11. By careful examination of the microstructures shown in images (a) and (b), one can easily say that the particles formed in both cases are nanorod-like crystals of HAp. However, the size of the HAp crystals grown under the two different conditions are quite changed. The diameter and length of the HAp nanorod-like crystals prepared without EDTA are ~20 and 200 nm, respectively. These dimensions have been found to be less than half

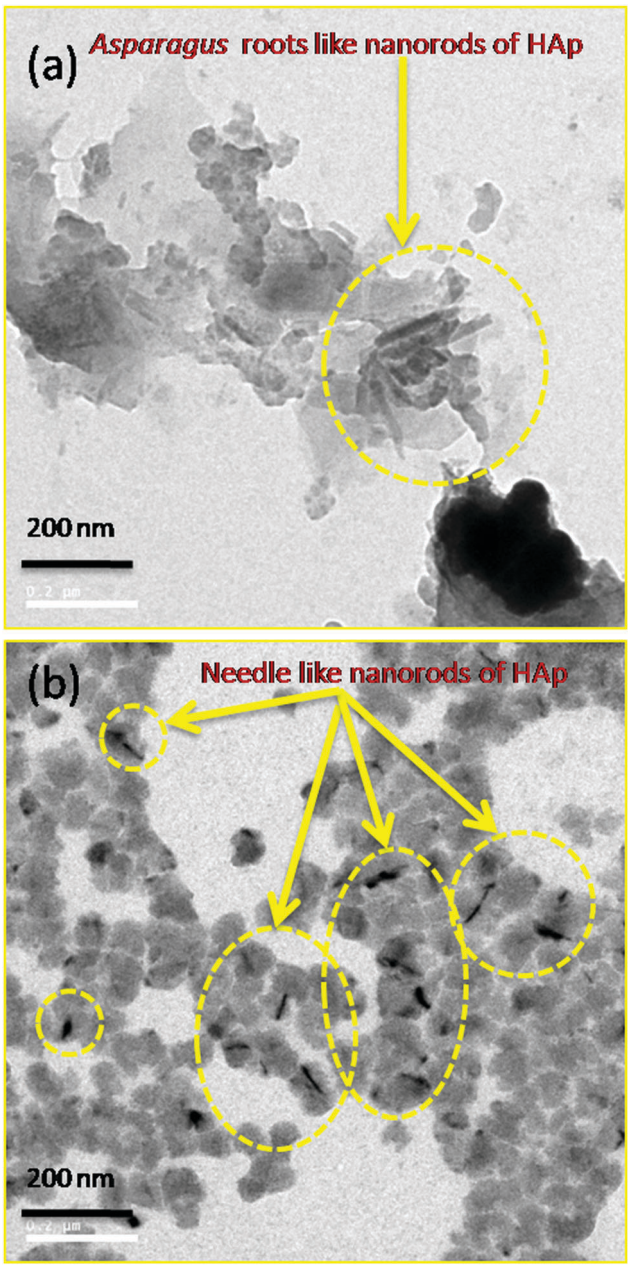

Fig. 8 TEM images of HAp powders prepared (a) without EDTA (b) using EDTA.

those observed for the EDTA assisted HAp nanorods. The diameter of the nanorods is ~10 nm and the length is less than 100 nm. An interesting fact revealed by the TEM characterization was that the nanorods in image (a) show *Asparagus* roots-like agglomeration marked by a dotted yellow ring. However, in image (b), the nanorods are scattered needle-like structures marked by several dotted yellow rings. Thus, it is confirmed that the capping agent (EDTA) prevents agglomeration as also concluded by SEM. The results extracted by the TEM micrographs are in good agreement with results of the SEM microstructures.

The final morphology of the HAp nanomaterials may be understood on the basis of the driving force governed by the surface energy of the particles; the surface energy was controlled by the physico-chemical conditions. Subsequently, the effect of the chemical conditions, pH and EDTA on the structural and optical characteristics of HAp was investigated and discussed below.

A very familiar fact is that when we break a large solid piece of material into smaller parts, it always needs energy to break the bonds between neighboring atoms and it generates new surfaces.[43] The driving force existing in the materials during their synthesis was to minimize the surface area; the smaller the surface to volume ratio of the particles, the lower the energy state of the material. In order to minimize the surface energy, the directed bonds in isotropic lattices increase crystallization into rods/strips or plates, *i.e.* formation of one- or two-dimensional particles.[44]

The solubility of a system depends on the pH of the solution. Therefore, it can affect the chemical precipitation and particle agglomeration in the presence of a complexing agent (EDTA). At the beginning, the pH of the starting solution was 4. As the pH of the solution was increased, the solubility of the system increases and the solution turned from a milky white color to colorless. At pH 9, the solution became totally transparent and clear. At the initial stages of the experiment (in the clear solution before microwave irradiation), a cluster with a critical size of HAp would be formed and it forms the nucleus for HAp crystal growth. The HAp nuclei grow into crystallites when the solution was subjected to microwave irradiation at a frequency of 2.45 GHz. The further growth of the HAp crystal was controlled totally by the stability of the Ca–EDTA complex and the presence of OH^- on the facets. Due to the poor stability of the Ca–EDTA complex at pH 9, the Ca^{2+} ions and EDTA are separated from each other. Now, due to ionic interactions, the surface of OH^- behaves as an active site for the absorption of Ca^{2+} ions. In fact at pH 9, there were two opposite facets of crystallite active with OH^- ions and the crystallites grow with an anisotropic structure of HAp under microwave treatment. Consequently, a preferred growth along the (002) axis of hexagonal HAp was observed in the X-ray diffraction (XRD) patterns resulting in an increased strip-like/rod-like morphology with larger average particle size.[45] As we increase the pH of the solution, the concentration of OH^- ions and stability of the Ca–EDTA complex increases. Therefore, Ca^{2+} and EDTA will not be separated from each other. Therefore, Ca and EDTA exist together in the form of the Ca–EDTA complex at higher pH values. Under these conditions, all the facets of the crystallite with a high specific surface energy were active at the same potential due to the strong adsorption of OH^- ions. These facets have an almost equal ability to attach with Ca in the form of Ca–EDTA due to the same concentration of OH^- on each facet. Thus, under these physical and chemical conditions, the space between neighboring Ca–EDTA complex molecules results in an arrangement of Ca atoms in a disordered state rather than the intrinsic crystal structure of HAp. During microwave irradiation, the absorbed Ca–EDTA complex decomposed at a temperature of around 200 °C. Under homogeneous and fast heating, the HAp was found to have a flower-like shape in the nanostructure due to the anisotropic growth of the HAp crystals. This follows that

the pH value of the final solution and the presence of a capping agent (EDTA) play a key role in the synthesis of the final nanostructure and its shape. Apart from these, the microwave power and duration of the on–off cycle also have important roles in the synthesis of the HAp nanostructures.

Though the chelating agent was desirable, it was not compulsory for the formation of HAp nanostructures. The template free growth of HAp nanorings having enhanced properties has been reported.[46] We emphasize that the formation of a specific nanostructured morphology in every instance was directly controlled by the driving force and that the surfactants were only incidental for the formation of such structures. Preliminary investigations show that two-dimensional morphologies can be obtained in several other systems, including ZnO without using a surfactant. We believe that the primary role of the surfactant was to provide size control in the formation of the two-dimensional structures. However, the role of the surfactant was critical for the shape-controlled synthesis of various three-dimensional morphologies such as cubes,[47] rods[48] and wires.[49] In the 1990s, Roy and co-workers synthesized and fabricated porous and transparent HAp ceramics using microwave processing and sintering.[50–52] It is important to note that the microwave energy corresponding to a frequency of 2.45 GHz is absorbed strongly by the bound water molecules in the hydration sphere of a polyvalent ion. This absorption of microwave power weakens the bonds between the calcium ion and its sphere of hydration, which was of paramount importance for the formation of apatite in aqueous solutions *via* facilitating the deaquation step[2] though the solid state synthesis of HAp *via* a microwave route was already established.[53]

4. Conclusions

In the present investigation, it is concluded that EDTA and pH play important roles to decide the morphology and structure of HAp. According to the IR spectroscopic results, carbonate impurities were absorbed probably from the atmosphere in the HAp samples during their synthesis and this could not be avoided under the normal synthesis conditions. However, this process can be reduced using a capping agent (EDTA). In the present study, EDTA plays a vital role for the formation of pure phase HAp nanostructures and prevents the incorporation of carbonate impurities. EDTA efficiently affects the morphology of the HAp nanostructures. Samples prepared in the absence of EDTA show agglomeration. TEM confirmed the role of EDTA. TEM exhibited the formation of HAP as scattered needle-like nanostructures without agglomeration. The particle size of HAp powder was found to be strongly dependent on the presence of EDTA. The particle size of the EDTA assisted HAp sample (diameter × length is 10 nm × 100 nm) as shown in TEM micrograph (b) was just half of that found for the HAp formed without EDTA (20 nm × 200 nm). Changes in pH also caused a large change in the morphology of the HAp powders. Needle-like nanostructures at pH 9 are reshaped into flower-like nanostructures at pH 13. By altering the chemical and/or physical preparation conditions, the desired morphology of HAp structures may be obtained. The HAp nanoparticles with sizes below 100 nm are extremely useful in specific site as well as normal drug delivery. FT-IR, LIBS, SEM and TEM techniques confirmed the formation of the HAp powders. These techniques confirmed the superiority of EDTA assisted HAp samples over the samples formed without EDTA.

Acknowledgements

V. K. Mishra is cordially thankful to the University Grants Commission, India for financial support in the form of Senior Research Fellowship in Science for Meritorious Students (SRF-UGC-RFSMS) (No. F.5-127/2007 (BSR) 15.03.2013). The authors are thankful to Prof. Ranjan K. Singh for the Raman measurements (Department of Physics, Banaras Hindu University), Prof. A. K. Rai (Department of Physics, Allahabad University) for the LIBS measurements and Prof. R. K. Mandal (IIT-BHU) for the TEM facilities.

Notes and references

1 L. L. Hench, *J. Am. Ceram. Soc.*, 1991, **74**, 1487.
2 A. Siddharthan, S. K. Seshadri and T. S. S. Kumar, *Scr. Mater.*, 2006, **55**, 175.
3 W. Suchanek, M. Yashima, M. Kakihana and M. Yoshimura, *Biomaterials*, 1996, **17**, 1715.
4 S. R. Radin and P. Ducheyne, *J. Biomed. Mater. Res.*, 1994, **28**, 1303.
5 J. C. Elliot, *Montpellier*, Sauramps Medical, London UK, 1998.
6 S. Aryal, K. C. R. Bahadur, N. Dharmaraj, K. W. Kim and H. Y. Kim, *Scr. Mater.*, 2006, **54**, 131.
7 Y. Huang, X. Zhang, R. Zhao, H. Mao, Y. Yan and X. Pang, *J. Mater. Sci.*, 2015, **50**, 1688.
8 Q. Ding, X. Zhang, Y. Huang, Y. Yan and X. Pang, *J. Mater. Sci.*, 2015, **50**, 189.
9 R. Murugan and S. Ramakrishna, *Cryst. Growth Des.*, 2005, **5**, 111.
10 F. Ye, H. Guo and H. Zhang, *Acta Biomater.*, 2010, **6**, 2212.
11 Y. Shinto, A. Uchida, F. Korkusuz, N. Araki and K. Ono, *J. Bone Jt. Surg., Br. Vol.*, 1992, **74**, 600.
12 S. H. Zhu, B. Y. Huang, K. C. Zhou, S. P. Huang, F. Liu, Y. M. Li, Z. G. Xue and Z. G. Long, *J. Nanopart. Res.*, 2004, **6**, 307.
13 P. Sibilla, A. Sereni, G. Aguiari, M. Banzi, E. Manzati and C. Mischiati, *J. Dent. Res.*, 2006, **85**, 354.
14 S. Dasgupta, A. Bandyopadhyay and S. Bose, *Acta Biomater.*, 2009, **5**, 3112.
15 T. Y. Liu, S. Y. Chen, D. M. Liu and S. C. Liou, *J. Controlled Release*, 2005, **107**, 112.
16 B. Palazzo, M. Iafisco, M. Laforgia, N. Margiotta, G. Natile, C. L. Bianchi, D. Walsh, S. Mann and N. Roveri, *Adv. Funct. Mater.*, 2007, **17**, 2180.
17 Y. P. Guo, Y. B. Yao, Y. J. Guo and C. Q. Ning, *Microporous Mesoporous Mater.*, 2012, **155**, 245.

18 V. K. Mishra, B. N. Bhattacharjee, O. Parkash, D. Kumar and S. B. Rai, *J. Alloys Compd.*, 2014, **614**, 283.
19 G. Bezzi, G. Celotti, E. Landi, T. M. G. L. Torretta, I. Sopyan and A. Tampieri, *Mater. Chem. Phys.*, 2003, **78**, 816.
20 S. Jadalannagari, S. More, M. Kowshik and S. R. Ramanan, *Mater. Sci. Eng., C*, 2011, **31**, 1534.
21 H. Zhang, S. Li and Y. Yan, *Ceram. Int.*, 2001, **27**, 451.
22 L. B. Kong, J. Ma and F. Boey, *J. Mater. Sci.*, 2002, **7**, 1131.
23 H. S. Liu, T. S. Chin, L. S. Lai, S. Y. Chiu, K. H. Chuang, C. S. Chang and M. T. Lui, *Ceram. Int.*, 1997, **23**, 19.
24 M. Toriyama, A. Ravaglioli, A. Krajewski, G. Celotti and A. Piancastelli, *J. Eur. Ceram. Soc.*, 1996, **16**, 429.
25 K. Itatani, K. Iwafune, F. S. Howell and M. Aizawa, *Mater. Res. Bull.*, 2000, **35**, 575.
26 P. Luo and T. G. Nieh, *Mater. Sci. Eng., C*, 1995, **3**, 75.
27 A. C. Tas, *J. Eur. Ceram. Soc.*, 2000, **20**, 2389.
28 S. Bose and S. K. Saha, *Chem. Mater.*, 2003, **15**, 4464.
29 M. Roy, A. Bandyopadhyay and S. Bose, *J. Am. Ceram. Soc.*, 2010, **93**, 3720.
30 V. K. Mishra, S. B. Rai, B. P. Asthana, O. Parkash and D. Kumar, *Ceram. Int.*, 2014, **40**, 11319.
31 V. K. Mishra, S. K. Srivastava, B. P. Asthana and D. Kumar, *J. Am. Ceram. Soc.*, 2012, **95**, 2709.
32 J. Liu, K. Li, H. Wang, M. Zhu and H. Yan, *Chem. Phys. Lett.*, 2004, **396**, 429.
33 A. Lak, M. Mazloumi, M. S. Mohajerani, S. Zanganeh, M. R. Shayegh, A. Kajbafvala, H. Arami and S. K. Sadrnezhaad, *J. Am. Ceram. Soc.*, 2008, **91**, 3580.
34 N. Y. Hsu and Y. W. Lin, *New J. Chem.*, 2016, **40**, 1155.
35 D. M. Roy and S. K. Linnehan, *Nature*, 1974, **247**, 220.
36 D. L. Goloshchapov, V. M. Kashkarov, N. A. Rumyantseva, P. V. Seredinn, A. S. Lenshin, B. L. Agapov and E. P. Domashevskaya, *Ceram. Int.*, 2013, **39**, 4539.
37 H. Monma and T. J. Kamiya, *Mater. Sci.*, 1987, **22**, 4247.
38 G. S. Maurya, A. Jyotsana, R. Kumar, A. Kumar and A. K. Rai, *Phys. Scr.*, 2014, **89**, 075601.
39 N. Ignjatovic, V. Savich, S. Najman, M. Plavsic and D. Uskokovic, *Biomaterials*, 2001, **22**, 571.
40 L. Li, Y. Liu, J. Tao, M. Zhang, H. Pan, X. Xu and R. Tang, *J. Phys. Chem. C*, 2008, **112**, 12219.
41 National Institute of Standards and Technology, ''Electronic database,'' http://physics.nist.gov/PhysRef Data/ASD/lines form.html.
42 Z. E. Erkmen, *J. Biomed. Mater. Res., Part B*, 1999, **48**, 861.
43 D. Vollath, *Nanomaterials: an introduction to synthesis, properties and applications*, WILEY-VCH Verlag GmbH and Co. KGaA, Weinheim-Germany, 2008.
44 H. Cao, L. Zhang, H. Zheng and Z. Wang, *J. Phys. Chem. C*, 2010, **114**, 18352.
45 E. S. Ahn, N. J. Gleason, A. Nakahira and J. Y. Ying, *Nano Lett.*, 2001, **1**, 149.
46 A. J. Nathanael, S. I. Hong, D. Mangalaraj, N. Ponpandian and P. C. Chen, *Cryst. Growth Des.*, 2012, **12**, 3565.
47 Y. Sun and Y. Xia, *Science*, 2002, **298**, 2176.
48 C. J. Murphy and N. R. Jana, *Adv. Mater.*, 2002, **14**, 80.
49 A. Halder and N. Ravishankar, *Adv. Mater.*, 2007, **19**, 1854.
50 Y. Fang, D. K. Agrawal, D. M. Roy and R. Roy, *J. Mater. Res.*, 1992, **7**, 490.
51 Y. Fang, D. K. Agrawal, D. M. Roy and R. Roy, *J. Mater. Res.*, 1994, **9**, 180.
52 Y. Fang, D. K. Agrawal, D. M. Roy and R. Roy, *Mater. Lett.*, 1995, **23**, 147.
53 J. M. Cao, J. Feng, S. G. Deng, X. Chang, J. Wang, J. S. Liu, P. Lu, H. X. Lu, M. B. Zheng, F. Zhang and J. Tao, *J. Mater. Sci.*, 2005, **40**, 6311.